1 Physical Mechanisms of Atomic-Scale Friction

Ya-Pu Zhao and Xueyan Zhu

CONTENTS

ABSTRACT

Friction is one of the fundamental problems of both theoretical and practical significance. The earliest laws of friction were established from experimental experience, which is on the macroscopic scale. Owing to the development of experimental techniques and simulation methods on the atomic scale, the mechanisms of friction are found to be closely related to the intermolecular

interactions at the interface. In addition, the basic laws of friction are found to be invalid at nanoscale where surface area forces play an important role. Here, we focus on the physical mechanisms and phenomena of friction from the point of view of atomic-scale interactions. The main discussion is devoted to the commensurate and incommensurate phases, several atomic-scale frictional models, the physical origin of velocity-dependent friction, and thermally diffusing friction, and some prospects are outlined.

1.1 INTRODUCTION

1.1.1 Dry Friction and Tribology

Friction is one of the oldest problems in physics and engineering, and one of the most important phenomena to everyday life. It is estimated that the losses in the U.S. economy due to friction total about 6% of the gross national product. Friction is even more important to micro- and nano-electromechanical systems (MEMS and NEMS) because these smaller systems are more affected by surface forces than larger systems.

The rigorous study of friction dates back to Leonardo da Vinci (1452–1519), the Italian Renaissance mathematician. Around 1480, da Vinci postulated that friction was proportional to load and independent of the area of the subject being moved, which is the well-known "da Vinci's two postulates" on friction. This was indeed a substantial step toward the establishment of basic friction laws. Figure 1.1 shows the sketches from da Vinci's notebook demonstrating some of his notable friction experiments. Unfortunately, da Vinci's two postulates on friction remained unpublished in his notebooks. Besides, da Vinci was the first to introduce the term "coefficient of friction." Two important statements by da Vinci's are: "The friction made by the same weight will be of equal resistance at the beginning of its movement although the contact may be of different breadth and length." and "Friction produces double the amount of effort if the weight be doubled."

In 1687, Sir Isaac Newton (1642–1727) studied the fluid properties that affected lubricated friction. Guillaume Amontons (1663–1705), the French scientific instrument inventor and physicist, enunciated da Vinci's two postulates in 1699, elevating

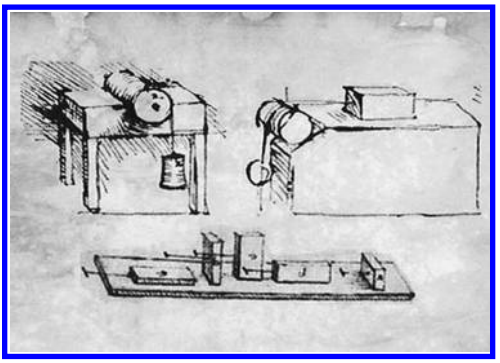

FIGURE 1.1 Sketches from da Vinci's notebook, ca. 1480 demonstrating his friction experiments.

them to "laws" [1], which were verified by the French physicist Charles-Augustin de Coulomb (1736–1806) in 1781. Also in 1781, Coulomb described experiments on sliding and rolling friction and formulated the third classic law of dry friction. In his investigation of friction, Coulomb combined quantitative experimental researches with mathematical analyses in a way that was highly unusual at the time, but that was characteristic of all his work. His paper was of immediate relevance to the engineering practice and his analysis became, for over a century, the starting point for all serious studies of friction. Of Coulomb, Thomas Young (1773–1829), the English mathematician, once wrote, "his moral character is said to have been as correct as his mathematical investigations."

The three basic laws of friction are summarized as follows:

- Amontons' 1st law: Friction force is directly proportional to the applied load.
- Amontons' 2nd law: Friction force is independent of the apparent area of contact.
- Coulomb's law: Kinetic friction is independent of the sliding velocity.

It should be noted that these three fundamental laws only apply to dry friction, in which the addition of a lubricant modifies the tribological properties significantly.

Modern scientific studies were conducted in the late 1930s by F.P. Bowden (1903–1968) and David Tabor (1913–2005) [2], who established a tribophysics laboratory for the CSIRO (The Commonwealth Scientific and Industrial Research Organisation) in Melbourne, Australia.

In 1964, H.P. Jost discussed with the editor of the *Oxford Dictionary of the English Language* about the term for this interdisciplinary field, and suggested to the editor that the Greek word "tribos"—rubbing—would seem appropriate. Thus, H.P. Jost coined the word "tribology" for "the science and technology of interacting surfaces in relative motion and associated practices."

1.1.2 Kinetic Friction

Leonard Euler (1707–1783), the great mathematician and physicist, introduced the difference between static frictional force and kinetic frictional force. He also introduced the Greek symbol μ as the coefficient of friction.

Kinetic friction occurs when two objects are moving relative to each other and rub together (like a sled on the ground). For most materials, kinetic friction is considerably smaller than static friction [3]. In 1939, Bowden and Leben [4] showed that during relative sliding there is an increase in temperature at sliding surfaces. This led to the idea that kinetic friction could be less than static friction because the temperature rise during rapid sliding may cause thermal softening of the material.

Kinetic friction is now understood, in many cases, to be primarily caused by chemical bonding between the surfaces, rather than interlocking asperities. However, in many other cases, roughness effects are dominant, such as in rubber to road friction. Surface roughness and contact area, however, do affect kinetic friction for micro- and nano-scale objects where surface area forces dominate inertial forces.

1.1.3 Atomic-Scale Friction

Friction is nonlinear [5], velocity-dependent [6], interface topography and chemical property sensitive [7,8], and multi-scale in nature.

Friction and wear can be very-severe problems for tiny objects and devices. MEMS and NEMS have very-high surface-to-volume ratios, which means that their surfaces quickly wear out or even spontaneously stick together as they come into contact. As shown in Figure 1.2 [9], wear is the primary failure mechanism for MEMS actuators that involve sliding motion. Scanning electron microscope (SEM) images of two microengine gears stressed under different humidity conditions 31% and 1.8% RH at 25°C are shown in Figure 1.3; the microengines were stressed for roughly the same number of cycles (600,000), but the amount of wear debris for each humidity was dramatically different [10]. The big problem of friction and wear in MEMS and NEMS devices may be attributed to adhesion, abrasion, corrosion, surface fatigue, deformation, impact and fretting wear. Due to the microscopic nature of these mechanisms, we must have a clear picture of friction at the atomic scale.

The mechanism of atomic friction, generally considered as first presented in 1929 by Tomlinson [11], was already used a year before by Prandtl [12] as a model for the dynamic of shift lines in a crystal [13,14]. This is why the first atomic friction model is generally termed as "Prandtl–Tomlinson Model."

Ludwig Prandtl (1875–1953), was a German scientist mostly famous in fluid mechanics, but submitted his PhD thesis on solid mechanics; his interest was in the irreversible transformations of non-monocrystal solid at that time. Because there is no hysteresis in ideal monocrystals between voltage and transformation, he was drawn to say that the dynamics of shift lines must be responsible for this phenomenon. His model of the behavior of an atom belonging to a shift line equaled the one of Tomlinson for a surface atom during the friction process. It is obvious that he could explain the hysteresis effects.

Prandtl visualized this system with a mechanical model consisting of a wave-like surface upon which a heavy roller rolls back and forth. As shown in Figure 1.4, the elastic force is realized by the springs whose ends are fastened to a gliding stage.

The Frenkel–Kontorova (FK) model [15,16], introduced by the Soviet physicist, Yakov Il'ich Frenkel (1894–1952) and his PhD student, T. Kontorova, is a harmonic

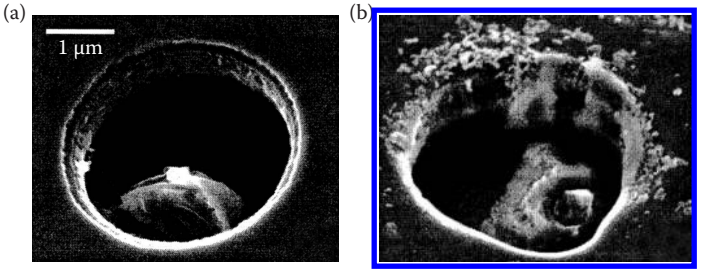

FIGURE 1.2 Wear-out of a pin hole of a micromachine. (a) normal pin hole; (b) wear-out pin hole. (Adapted from W M Miller et al. *Proceedings of 4th Annual "The Reliability Challenge*," Dublin, Ireland, pp. 4.1–4.7, 1998.)

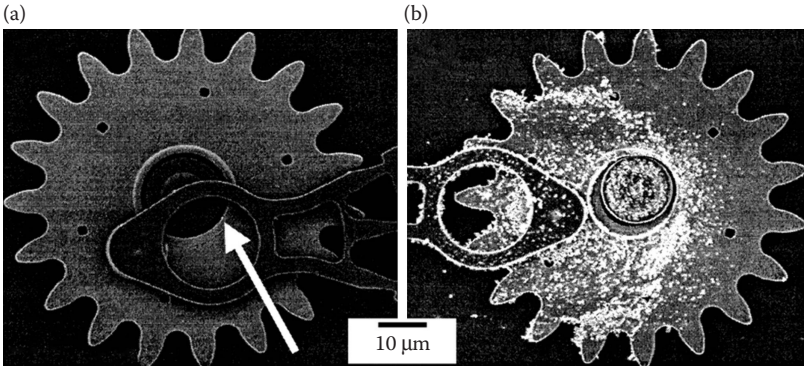

FIGURE 1.3 SEM images [10] of two microengine gears stressed under different humidity conditions at 25°C. The microengines were stressed for roughly the same number of cycles (600,000), but the amount of wear debris for each humidity was dramatically different. (a) 31% RH; (b) 1.8% RH. (Adapted from D M Tanner et al., *Proceedings of IEEE International Reliability Physics Symposium*, San Diego CA, pp. 189–197, 1999.)

chain (mimicking a layer of atoms) in a spatially periodic potential (mimicking the substrate). The chain is driven by a constant force that is damped by a velocity-proportional damping (emitting waves into the substrate). The FK model is one of the most simple and richest models of nanotribology and classical mechanics [16,17]. The nonlinearity of this model leads either to the exactly integrable Sine-Gordon equation which could introduce topological and dynamical solutions, or to the important equation of stochastic theory, the Taylor–Chirikov map, which involves such issues as fractal structures, commensurate–incommensurate (C–I) transitions, glass-like behavior, and so on. The FK model describes a variety of physical objects such as dislocations in solids, domain walls (DWs), Josephson junctions, biological molecules, and crystal surfaces.

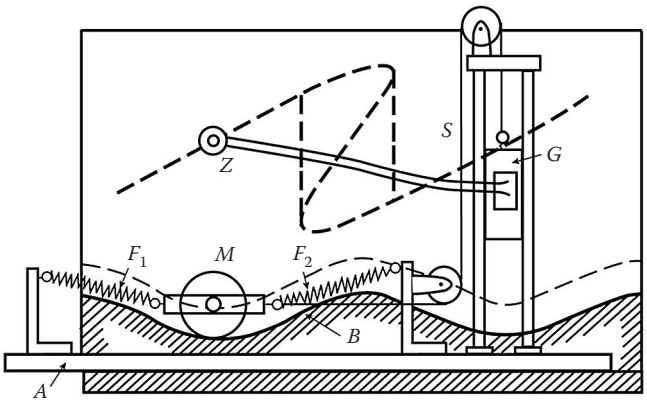

FIGURE 1.4 Prandtl's visualization of the Tomlinson mechanism in 1928. (Adapted from L Prandtl. *Zeitschrift für Angewandte Mathematik und Mechanik*, 8, 85–106, 1928.)

1.1.4 A Generalized Classification of Friction Laws

The various friction laws can be roughly grouped into four types [7]: (1) friction laws based on macroscale theories including Amontons' law, and the model due to Bowden and Tabor; (2) laws based on single-asperity theories including both nonadhesive and adhesive contacts; (3) laws based on multi-asperity theories including both nonadhesive and adhesive contacts; (4) laws based on atomic-friction models discussed in Section 1.1.3. These friction laws are summarized in Table 1.1.

1.1.5 Some Recent Research Progress on Atomic-Scale Friction

1.1.5.1 Nanoscale Friction and Wear Maps

The components used in MEMS and NEMS are of the order of a few micrograms, and operate under loads of the order of a few micrograms to a few milligrams. With the miniaturization from macro- to nanoscale, the surface-to-volume ratios increased

TABLE 1.1
Generalized Classification of Friction Laws

Friction Laws	F_f versus Area	F_f versus L	Notes
	Macroscale Theories		
Amontons' law	Independent of A_{macro}	$F_f = \bar{\mu} \cdot L$	Law first discovered by Leonardo da Vinci
Bowden and Tabor	$F_f = \bar{\tau} \cdot \Sigma A_{asp}$	$F_f = \bar{\mu} \cdot L$	Law results from contact roughness
	Single-Asperity Theories		
Nonadhesion (based on Hertz model)	$F_f = \tau \cdot A_{asp}$	$F_f \sim L^{2/3}$	Linear dependence of F_f on A_{asp} is generally believed to be true for microscale contacts, but has been questioned for nanoscale contacts
Adhesive (e.g., Maugis–Dugdale)	$F_f = \tau \cdot A_{asp}$	Sublinear	
	Multi-Asperity Picture of Nanoscale Contact (Our Model)		
Nonadhesive	$F_f = \tau \cdot A_{real} = \tau \cdot N_{at} \cdot A_{at}$ $F_f \neq \tau \cdot A_{asp}$	$F_f = \mu \cdot L$	Dependence of F_f on A_{real} has been directly verified. Linear dependence of F_f on L is due to atomic roughness and small contact pressures
Adhesive	$F_f = \tau \cdot A_{real} = \tau \cdot N_{at} \cdot A_{at}$ $F_f \neq \tau \cdot A_{asp}$	Sublinear	Adhesion induces transition from linear to sublinear behavior

Note: A_{macro} is the macroscopic contact area. A_{asp} is the contact area of a single asperity; A_{real} is the real contact area defined as the number of atoms N_{at} in contact multiplied by the average contact area A_{at} of an interfacial atom.

Source: With permission from Macmillan Publishers Ltd., *Nature*, Y F Mo, K T Turner and I Szlufarska. Friction laws at the nanoscale, 457, 1116–1119, copyright 2009.

considerably and became a cause of serious concern from the tribological point of view. On micro- and nanoscales, surface forces, such as friction, adhesion, meniscus forces, viscous drag and surface tension, which are proportional to area, significantly increase and can limit the life and reliability of nanotechnology devices. Tambe and Bhushan [18,19] proposed nanoscale friction and wear maps as shown in Figures 1.5 and 1.6.

Nanoscale friction and wear mapping can help identify some "sweet spots" that would give ultralow friction and near-zero wear [18]. Friction and wear at a sliding interface depend on the operating conditions such as normal load and sliding velocity; material properties such as Young's modulus and hardness; environmental conditions such as humidity and the medium to which the interface is exposed, such as air, a specific gas, or simply water; and interface properties such as surface roughness and surface energy. Many of the commonly observed friction and wear mechanisms are shown in Figure 1.6 [19]. Mapping nanoscale friction and wear as a function of operating conditions and interface properties is a valuable tool and has the potential to impact the very way in which we design and select materials for nanotechnology applications.

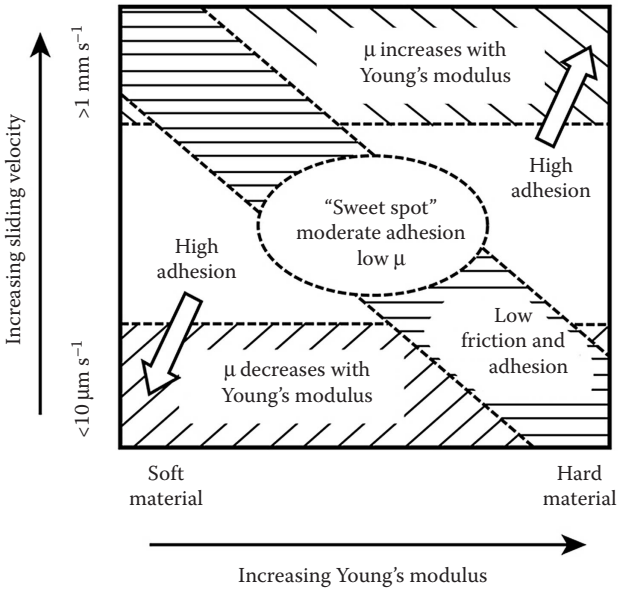

FIGURE 1.5 Map for identifying tribologically ideal materials with low friction and adhesion. At low velocities (less than 10 μm/s), the coefficient of friction (μ) decreases logarithmically with Young's modulus. At high velocities (more than 1 mm/s), μ increases with an increase in Young's modulus. The "sweet spot" corresponds to materials with low μ and moderate adhesion. The ideal zone for material selection is, however, the one where both μ and adhesion are either low or moderate and is the shaded diagonal portion. (With permission from N S Tambe and B Bhushan. Identifying materials with low friction and adhesion for nanotechnology applications. *Appl. Phys. Lett.*, 86, 061906. Copyright 2005, American Institute of Physics.)

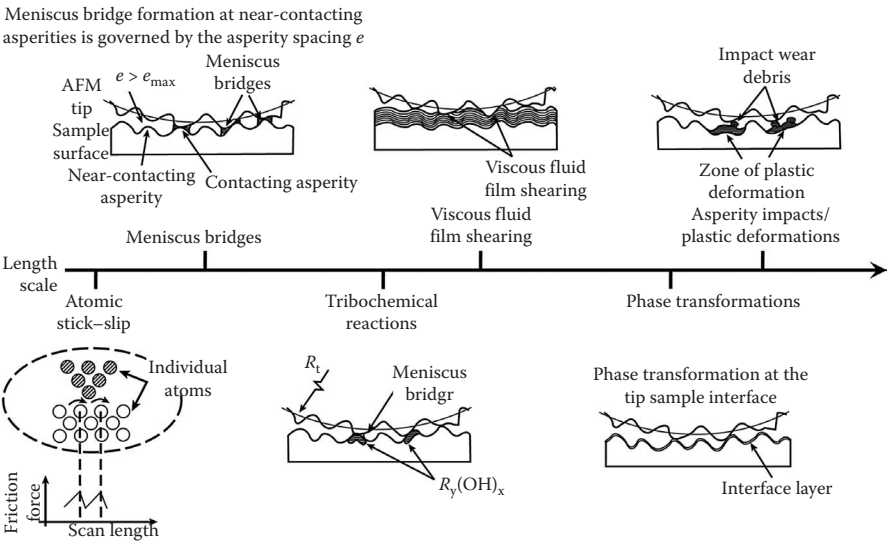

FIGURE 1.6 Most commonly observed mechanisms of friction and wear: nanoscale and macroscale. (Adapted from N S Tambe and B Bhushan. *Philos. Trans. R. Soc. A-Math. Phys. Eng. Sci.*, 366, 1405–1424, 2008.)

1.1.5.2 Atomic Friction between AFM Tip and Carbon Nanotube

To provide a better understanding of fundamental friction issues at atomic scale and offer a new tool for assembling carbon nanotubes (CNTs) into devices and clarifying the forces acting on them, Riedo and collaborators [20] reported the measurement of different friction forces when an atomic force microscope (AFM) tip slides the CNT along its axis compared to when the AFM tip slides perpendicular to its axis, as shown in Figure 1.7. This friction difference has its origins in soft lateral distortion of the nanotubes when they slide in the transverse direction. Asymmetries in the friction could potentially also be used in sorting CNTs according to their chirality, a property that is currently difficult to measure by other means.

As shown in Figure 1.8, when an AFM tip was scanned transversely across a multi-walled CNT, the amount of friction measured was twice as large as when the same nanotube was scanned longitudinally, along the length of the tube. The authors attributed this difference to what they call "hindered rolling"—that is, the additional effort required to overcome the nanotube's tendency to roll as the AFM tip strokes across it rather than along it. Because the energy required to move in one direction was twice as large as that required to move in the other direction, this could be an easy way to control the assembly of CNTs for nanoelectronics, sensors, and other applications. To assemble nanotubes on a surface, one needs to know how they interact and what force is needed to move them. Though friction has been studied before in nanotubes, this research was the first to provide detailed information about the frictional forces at work in both the longitudinal and transverse directions when the nanotubes interact with an AFM tip.

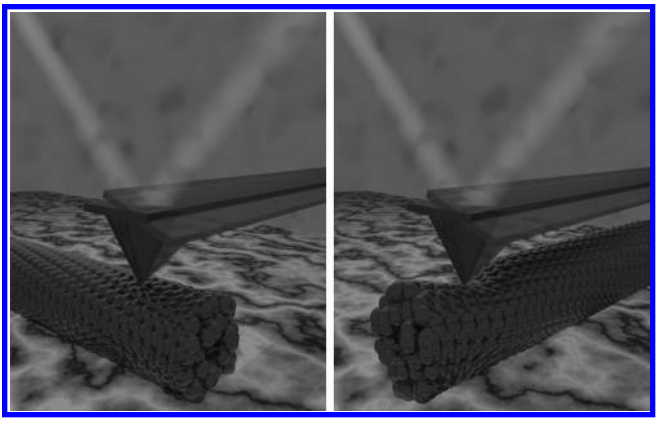

FIGURE 1.7 Images compare what happens when an AFM tip slides longitudinally along a carbon nanotube (left) versus when it slides across a nanotube transversely. (Adapted from M Lucas et al. *Nat. Mater.*, 8, 876–881, 2009.)

At the nanoscale, the frictional force F_F is proportional to the shear strength τ (in N/m^2) and the contact area A (in m^2):

$$F_F = \tau \cdot A \cdot (F_N + F_{adh}), \tag{1.1}$$

where F_N and F_{adh} are the normal force and the adhesion force between the AFM tip and the CNT. The friction force can also be written via the friction coefficient μ as

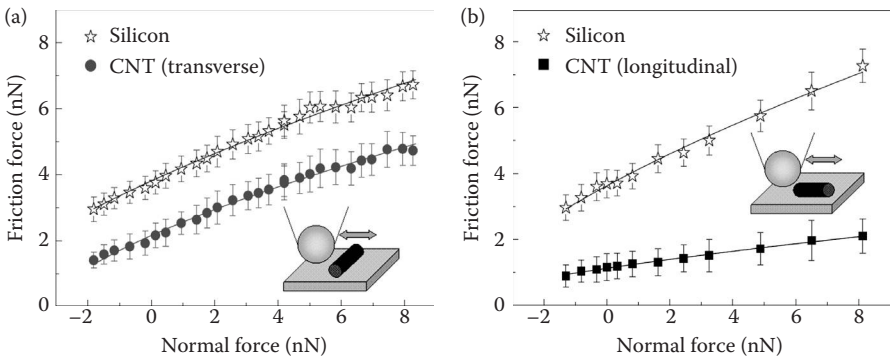

FIGURE 1.8 Frictional forces for transverse and longitudinal sliding. Frictional force as a function of the normal load for silicon and for transverse (a) and longitudinal (b) sliding on top of a CNT. The CNT radius is ~3.5 nm in the longitudinal section and ~5 nm in the transverse section. The sliding velocity was 0.8 μm/s. The solid lines are fits to the data using $F_F = \tilde{\mu} \cdot (F_N + F_{adh})^{2/3}$. The error in F_F is caused from the fluctuations in the values of friction in the investigated areas on top of the nanotubes. (With permission from Macmillan Publishers Ltd., *Nat. Mater.*, M Lucas et al., Hindered rolling and friction anisotropy in supported carbon nanotubes. 8, 876–881, copyright 2009.)

$$F_F = \mu \cdot (F_N + F_{adh}). \tag{1.2}$$

The contact area between a spherical tip (AFM tip) and a cylinder (CNT) or a flat surface (silicon substrate) can be expressed as a function of F_N, F_{adh}, elastic moduli, tip radius, R_{tip}, and cylinder radius, R_{NT}, by using continuum mechanics theories, such as the Hertz theory. As a result, one obtains

$$F_F = \tilde{\mu} \cdot (F_N + F_{adh})^{2/3}, \tag{1.3}$$

where $\tilde{\mu}$ is the nominal friction coefficient at the nanoscale. The measured shear strength and the adhesion force in this experiment are shown in Figure 1.9.

The experiment showed that greater forces were required to move the tip in the transverse direction. Using molecular dynamics (MD) simulations shown in Figure 1.10, the authors analyzed the phenomenon to understand what was happening. The simulation results are illustrated in Figure 1.11. For the MD simulation, there are three types of interactions [20]: the substrate–nanotube interaction, the interaction among the CNT atoms, and the nanotube–AFM tip interaction. For the substrate–nanotube interaction, the Au-C Lennard-Jones (LJ) potential [21] was used with the strength decreased by a factor of 10:

$$V_{Au\text{-}C}(r) = \frac{4\varepsilon_{Au\text{-}C}}{10}\left[\left(\frac{\sigma_{Au\text{-}C}}{r}\right)^{12} - \left(\frac{\sigma_{Au\text{-}C}}{r}\right)^{6}\right], \tag{1.4}$$

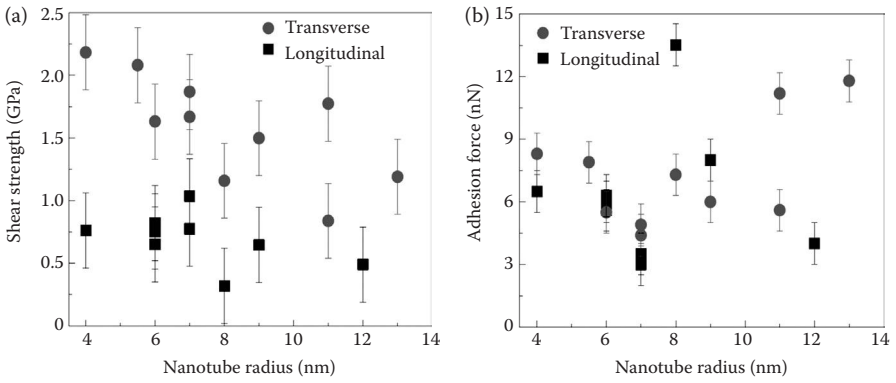

FIGURE 1.9 Shear strength and adhesion force. (a) Shear strength and (b) adhesion force for transverse and longitudinal sliding on top of a CNT as a function of the tube external radius. The sliding velocity was 2 μm/s for all of these measurements. The error in the shear strength is determined by fitting F_F versus F_N with Equation 1.1. The error in the adhesion force is obtained by the fit of F_F versus F_N with Equation 1.2. (With permission from Macmillan Publishers Ltd., *Nat. Mater.*, M Lucas et al., Hindered rolling and friction anisotropy in supported carbon nanotubes. 8, 876–881, copyright 2009.)

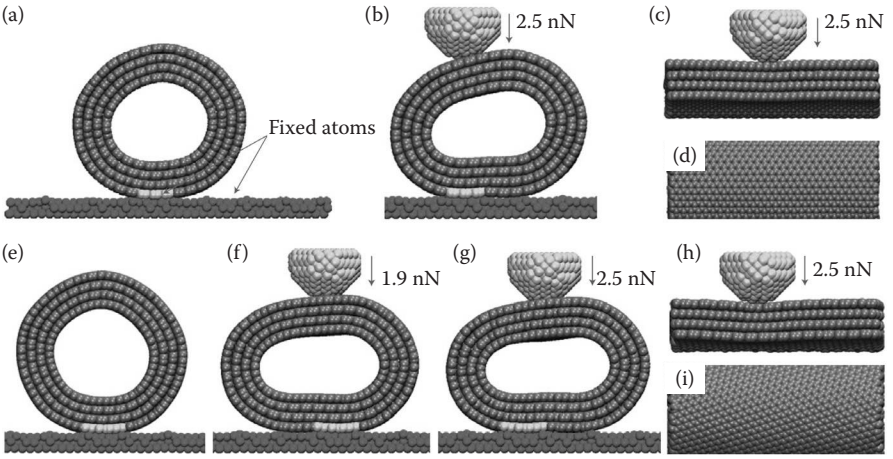

FIGURE 1.10 MD simulations of the tip-nanotube interaction. (a–b) Non-chiral tube without tip (a) and under 2.5 nN normal force (b). (c) The sectional view of the dimple. (d) View of the outer tube (armchair). (e–g) Chiral tube without tip (e) and under 1.9 nN (f) and 2.5 nN (g) with the tip pressing on two different spots. (h) Sectional view, under 2.5 nN. (i) Outer view of the chiral outer tube. (With permission from Macmillan Publishers Ltd., *Nat. Mater.*, M Lucas et al., Hindered rolling and friction anisotropy in supported carbon nanotubes. 8, 876–881, copyright 2009.)

where $\varepsilon_{\text{Au-C}}$ (in eV) is the potential well depth and $\sigma_{\text{Au-C}}$ (in nm) the distance at which the LJ potential is zero.

The interaction among the CNT atoms was modeled by the empirical Brenner potentials [22] and Kolmogorov–Crespi (KC) potentials [23]. The empirical Brenner potential is a kind of many-body potential that can model chemical bonding and the expression is

$$E_b = \sum_i \sum_{j(>i)} \left[V_R(r_{ij}) - \bar{B}_{ij} V_A(r_{ij}) \right], \tag{1.5}$$

where $\bar{B}_{ij}$ is a many-body coupling between the bond from atom i to atom j and the local environment of atom i, $V_R(r_{ij})$ and $V_A(r_{ij})$ represent pair-additive repulsive and attractive interactions, respectively. The KC potential is especially developed for the interlayer interaction in graphitic structures:

$$\begin{cases} V\left(\vec{r}_{ij}, \vec{n}_i, \vec{n}_j\right) = e^{-\lambda(r_{ij}-z_0)} \left[C + f(\rho_{ij}) + f(\rho_{ji}) \right] - A \left(\dfrac{r_{ij}}{z_0} \right)^{-6} \\ \rho_{ij}^2 = r_{ij}^2 - (\vec{n}_i \cdot \vec{r}_{ij})^2,\ \rho_{ji}^2 = r_{ij}^2 - (\vec{n}_j \cdot \vec{r}_{ij})^2 \\ f(\rho) = e^{-(\rho/\delta)^2} \sum C_{2n} \left(\dfrac{\rho}{\delta} \right)^{2n} \end{cases}, \tag{1.6}$$

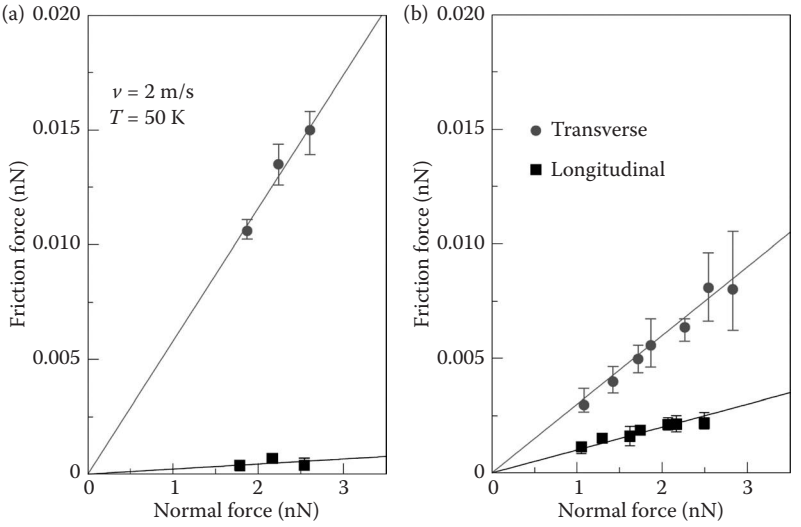

FIGURE 1.11 MD simulation of tip–nanotube friction force versus normal load. The tip slides back and forth with a speed v ~ 2 m/s. During the whole process, the temperature was set at $T = 50$ K to avoid large fluctuations of the frictional force related to the small CNT sizes. (a) Non-chiral nanotube (very large transverse–longitudinal anisotropy). (b) Chiral nanotube (more realistic transverse–longitudinal anisotropy of about 2). The friction–load behavior is to a good approximation linear (solid lines) and not a (2/3) power law as in the experiments, as the small size of the simulated tip and of the tip–CNT contact makes continuum contact mechanics invalid in this limit. Simulated friction extrapolates to zero at zero load, because the experimental zero-load situation corresponds to a finite load in the theory, the difference between the two corresponds to the experimental tip pull-off force, which measures adhesion, omitted in the simulation. The error bars indicate the friction fluctuations between different sliding loops. (With permission from Macmillan Publishers Ltd., *Nat. Mater.*, M Lucas et al., Hindered rolling and friction anisotropy in supported carbon nanotubes. 8, 876–881, copyright 2009.)

where f is introduced to reflect the directionality of the overlay, ρ the transverse distance, $\vec{n}_k$ the vector normal to the sp^2 plane in the vicinity of atom k.

For the nanotube–AFM tip interaction, the potential was assumed to only include the repulsive part of the LJ potential

$$V(r) = 4\varepsilon\frac{\alpha}{r}, \tag{1.7}$$

with $\varepsilon = 0.004$ eV and $\alpha = 0.328$ nm.

In principle, there seems to be no reason why the frictional forces required to move the AFM tip would be different in a particular direction. But the MD simulation confirmed that this "hindered rolling" and soft mode movement of the nanotubes were the sources of the higher friction when the tip moves transversely. Because the

nanotube-tip system is so simple, it offers an ideal platform for studying basic friction principles, which are important to all moving systems. This kind of system provides the opportunity to explore friction using an ideal experiment so one can really probe the energy dissipation mechanism.

Based on the MD simulations, the authors believed that the friction anisotropy will be very different in chiral nanotubes versus nonchiral—left-to-right symmetric—nanotubes. Because of the chirality, the tip moves in a screw-like fashion, creating hindered rolling even for longitudinal sliding. Thus, the new measuring technique may suggest a simple way to sort the nanotubes. Among the next steps in the research will be to show experimentally that this can be done.

An anisotropy in the friction coefficient of carbon nanotubes in the transverse and longitudinal directions has been shown, which has its origin in the soft lateral distortion of nanotubes when the tip–nanotube contact moves in the transverse direction. These findings could help in developing better strategies for chirality sorting, large-scale self-assembling of nanotubes on surfaces, and designing nanotube adhesives and nanotube–polymer composite materials.

1.2 COMMENSURATE AND INCOMMENSURATE INTERFACES, AND THEIR INFLUENCE ON TRIBOLOGY

It has been recognized that in the case of dry friction the rubbing surfaces exposed to air would be with a lubricant film inbetween, which is no more than a few monomolecular layers thick. Thus, many problems in tribology should be closely related to the structures of the rubbing surfaces and adsorbed lubricant film and corresponding registry of between these layers.

1.2.1 A One-Dimensional Case of Commensurate and Incommensurate Interfaces

As shown in Figure 1.12 [24], an array of atoms connected with harmonic springs interact with a periodic potential of period b, which is also known as the Frank and van der Merwe model [25]. In the context of friction, the particles represent the atoms of a sliding body. They are connected to each other through the springs that describe the bonds between the atoms. The periodic potential represents the effect of the solid substrate on the atoms of the sliding body. This could be a scenario of interacting gas atoms adsorbed on a crystalline substrate.

For the ratio between the unextended equilibrium length of the chain (a_0) and the period of the external potential (b), a_0/b, a distinction between two classes can be made. If this ratio is a rational number, the case is called *commensurate*; if the ratio is an irrational number, then the case is called *incommensurate*. From a practical point of view, the incommensurate case is the most interesting, because for two arbitrary surfaces making contact, a finite periodicity of the system is not likely.

Despite its extreme simplicity the model exhibits most of the features to be discussed in the following. Suppose the particles are immobile, the Hamiltonian of the

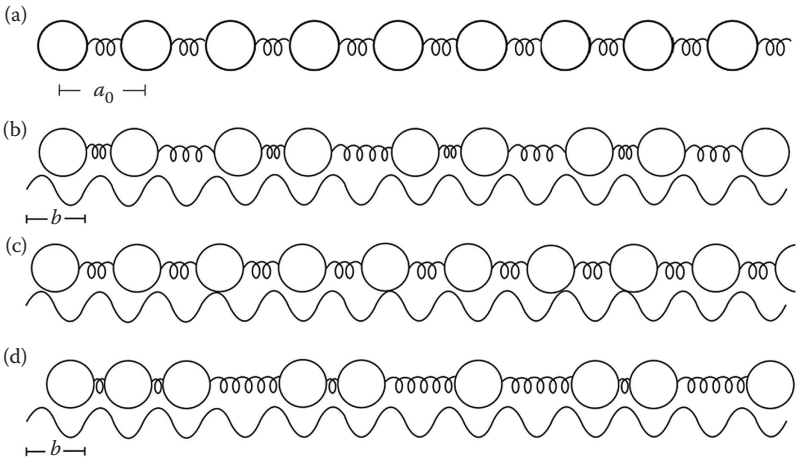

FIGURE 1.12 The one-dimensional Frank–van der Merwe model. The springs represent interactions between atoms, the wavy line the periodic potential. (a) Without the external potential, the spring length would favor a lattice constant a_0. (b–d) With external potential, the interaction between the chain and the substrate would force the system to form (b) commensurate structure, (c) incommensurate structure, or (d) chaotic structure. (Adapted from P Bak. *Rep. Prog. Phys.*, 45, 587–629, 1982.)

system consists of only the potential energy and may be written as the following dimensionless form:

$$H = \underbrace{\frac{1}{2b^2}\sum_n (x_{n+1} - x_n - a_0)^2}_{\text{elastic energy stored in the spring between particles of the chain}} + \underbrace{V\left[1 - \cos\left(\frac{2\pi}{b}x_n\right)\right]}_{\text{potential energy of the particles in the periodic external potential}}, \tag{1.8}$$

where x_n is the position of the nth atom. In the absence of the dimensionless periodic potential, V, the harmonic term would favor a lattice constant a_0 which in general, would be incommensurable with b: the adsorbed lattice forms an *incommensurate* structure as shown in Figure 1.12c. If the potential is strong enough it may be favorable for the lattice to relax into a *commensurate* structure where the average lattice spacing, a, is a simple rational fraction of the period b. Figure 1.12b shows a situation where $2a = 3b$.

Even in the case where the potential is not strong enough to force the chain into commensurability, the potential will always modulate the chain. The atoms will move toward the minima. The average period may approach a simple commensurate value, but remain incommensurate. In the most general incommensurate structure the position of the nth atom may be written as

$$x_n = na + \alpha + f(na + \alpha), \tag{1.9}$$

where α is a phase and f is continuous and periodic with period b. Here, a is the average distance between atoms (which in general is different from a_0) and f represents the modulation of the chain due to the potential. Since the energy does not depend on α, the chain is not locked to the potential.

Besides the commensurate and incommensurate structures, there are additional chaotic structures as shown in Figure 1.12d. The chaotic structure cannot be described by Equation 1.9 [24]. Consider, for instance, the situation where the potential is very strong compared with the elastic term. Clearly, there exist metastable configurations where the atoms are distributed in a random way among the potential minima. The chaotic phase is "pinned" to the potential. In contrast to the incommensurate phase, it is not possible to shift the lattice without climbing a potential barrier. In this respect the chaotic phase is similar to the commensurate phase, although the average period is, in general, incommensurate with the potential. If the atoms were charged, the incommensurate phase would be conducting and the chaotic phase insulating [26,27].

Similar to the bulk phase, the adsorbed atoms may experience phase transitions when the external conditions are varied. For example, the periodicity, a (or wavevector $q = 2\pi/a$), would change as the natural periodicity a_0 is varied. As shown in Figure 1.13, various possible situations for the change of q shall be encountered when the parameter x goes from x_1 to x_2. Figure 1.13a shows that the periodicity passes through an infinity of commensurate values without locking; such a system is called the "floating" phase. Figures 1.13b and 1.13c illustrate that the value of $q/2\pi$ could remain constant and rational at an infinity of finite intervals of the argument x, reflecting infinite commensurate values with locking, and the stability intervals decrease rapidly as the order of the commensurability increases. If the measure of

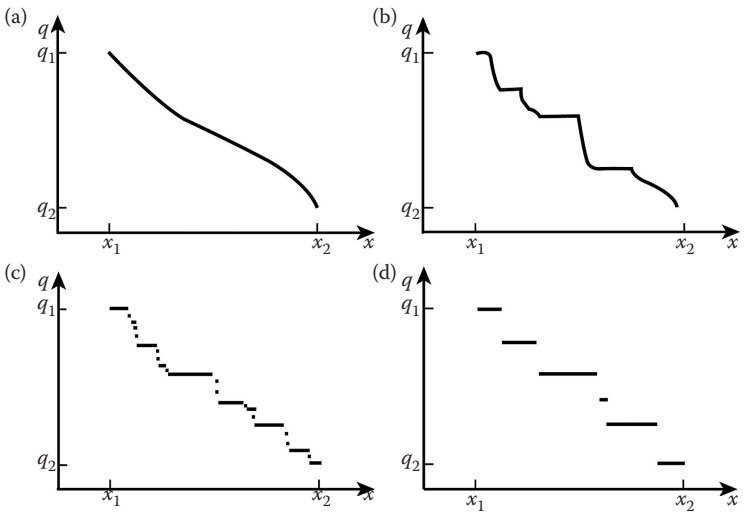

FIGURE 1.13 Variation of the inverse period, or wavevector q with parameter x, which could represent temperature, pressure, etc. (a) Smooth analytic behavior, (b) incomplete devil's staircase, (c) complete devil's staircase, (d) harmless staircase. (Adapted from P Bak. *Rep. Prog. Phys.*, 45, 587–629, 1982.)

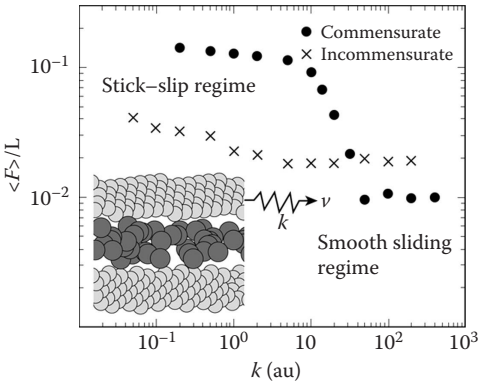

FIGURE 1.14 Kinetic friction force F_k divided by load L as a function of spring constant k for commensurate and incommensurate walls lubricated by a quarter layer. A schematic of the simulation is shown as well, in which the two surfaces slide relative to each other with velocity v. (With permission from M H Müser, *Phys. Rev. Lett.*, 89, 224301. Copyright 2002 by the American Physical Society.)

the incommensurate phases is not zero, the function is called "the incomplete devil's staircase" (Figure 1.13b). If the measure of the commensurate phases is zero, the function is called "the complete devil's staircase" (Figure 1.13c). Figure 1.13d is the "harmless staircase" where q assumes only a finite number of rational values.

Müser studied the nature of mechanical instabilities and their effect on kinetic friction from the point of view of dimensionality and commensurability [28]. It has long been recognized that kinetic friction F_k between two solids must be due to instabilities, that is, sudden "pops" of certain degrees of freedom. Here, such pops are studied with a focus on boundary lubrication. The pops' characteristics and, consequently, the friction–velocity relationship depend qualitatively on dimensionality, commensurability, and details of the lubricant–wall interaction. It is found that F_k should be small between commensurate surfaces. F_k is large for incommensurate surfaces, unless the lubricant's motion is confined to 1D (Figure 1.14). Müser discussed the effects of thermal noise, and employed computer simulations to show the relevance of the predictions to less idealized models [28].

1.2.2 A Two-Dimensional Case

Although some aspects of tribology have been obtained by studying the one-dimensional (1D) case of commensurate and incommensurate interfaces, some new aspects are revealed when the two-dimensional (2D) cases are considered. One of the important new aspects of the 2D system is that now not only the $T = 0$ ground state but also the $T \neq 0$ equilibrium state may be ordered exhibiting a number of different phases and phase transitions between them (T representing temperature) [17]. Recent decades have brought an immense amount of information on the rich variety of 2D phases that are formed on surfaces under various experimental conditions [29]. These include 2D gases (and lattice gases), liquids, crystals, liquid crystals, as well

as phases with an extended short-range order, which is specific of the 2D state only [30,31]. The structure of the adsorbed 2D phase is determined by the competition between particle–substrate interactions and particle–particle interactions. Here, the particle refers to the molecules or atoms adsorbed on the substrate.

As two adsorbed molecules come close to one another and their electronic shells overlap, they would interact according to the dipole–dipole mechanism which is long range [32]. This interaction is repulsive if their dipole moments are oriented parallel to each other (this is the case when the adsorbed molecules are chemically identical) and attractive if the dipole moments are antiparallel (e.g., in the case of interaction of an electropositive adsorbed molecule with an electronegative one). It shall be noted that there exists basic difference between the structures formed in the cases of attractive (Figure 1.15a) and repulsive lateral interactions (Figure 1.15b). To characterize the concentration of the adsorbed molecules on the surface, we introduce the value of degree of coverage, which is defined as $\theta = n/n_m$, where n is the surface concentration of the adsorbed molecules and n_m is their concentration in a close-packed monolayer.

For the attractive interactions, molecules tend to gather even at low coverage $\theta \ll 1$ (Figure 1.15a). When critical coverage is attained, a first-order phase transition starts, usually resulting in a structure commensurate with the substrate structure. However, if the attraction of the adsorbed molecules to the substrate is intense and if it is due to the difference of adsorbate and substrate atom radii, the packing of the first monolayer may continue and C–I phase transition would occur. The C–I transition starts with local breaking of commensurability between the adlayer and the substrate [33,34]. This occurs through formation of incommensurate regions (DWs) between the commensurate domains (Figure 1.16a). The elementary configurational excitation of the DW is a pair of oppositely oriented kinks as shown in Figure 1.16b.

The phase diagrams of adlayers with repulsive lateral interactions are more diverse than those described above (Figure 1.15b). First, phases with large interatomic distances are formed at low coverage degrees. Then, the first-order phase transition also

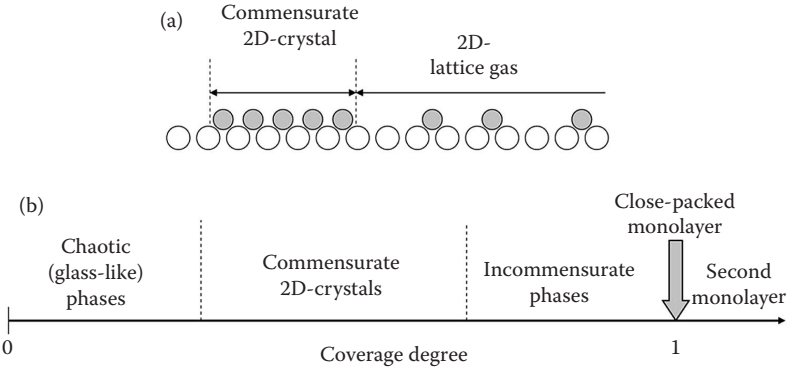

FIGURE 1.15 Possible scenarios of monolayer formation. (a) Two-dimensional condensation of attracting adparticles. (b) Structural states in the coverage degree range $0 < \theta < 1$ in the case of lateral repulsion. (From *Surf. Sci. Rep.*, 60, O M Braun and A G Naumovets, Nanotribology: Microscopic mechanisms of friction, 79–58, copyright 2006, with permission from Elsevier.)

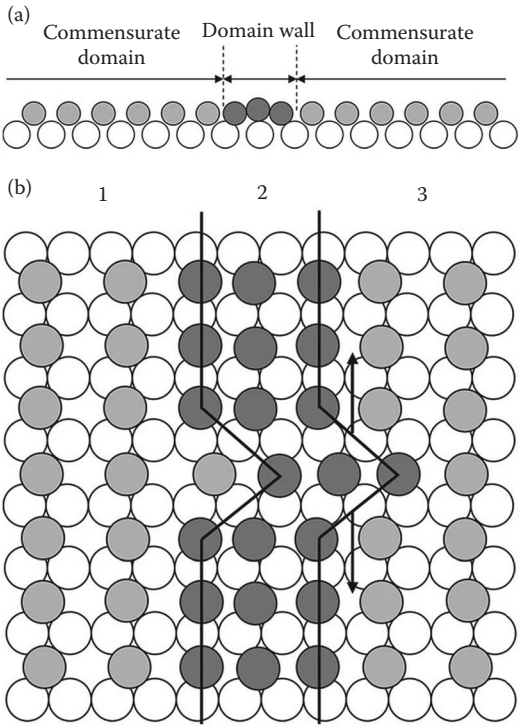

FIGURE 1.16 (a) A DW between two commensurate domains. (b) Model of a domain wall with kinks in the $p(1 \times 2)$ commensurate structure. Regions 1 and 3 are the commensurate $p(1 \times 2)$ domains while region 2 is the soliton. (From *Surf. Sci. Rep.*, 60, O M Braun and A G Naumovets, Nanotribology: Microscopic mechanisms of friction, 79–158, copyright 2006, with permission from Elsevier.)

occurs, which is attributed to progressive reduction of the amplitude of the repulsive interaction as the adlayer density increases. Some systems may even undergo a few first-order phase transitions within the coverage range $0 < \theta < 1$. The interpretation of this phenomenon should take into account the indirect interaction of the adsorbed molecules, whose energy oscillates with distance. This imposes a discrete set of distances at which the adsorbed molecules can arrange themselves on the surface.

Robbins and coworkers [8,35,36] and Müser and Robbins [37] found that the static friction originates from the commensurateness between the adlayer and the rubbing surface. They demonstrated that adsorbed monomers could change the static friction from zero to a finite value. The nature of friction comes from the intermolecular interactions. When the adlayer is commensurate with the substrate, their potential surfaces would be in registry with each other. Thus, the potential barrier should be overcome for relative movement between the adlayer and the substrate, leading to an abrupt increase of friction.

When two surfaces come in direct contact with each other, friction appears only occasionally. Krim and coworkers measured no static friction between substrates and incommensurate adsorbed layers [38,39], which is also consistent with results

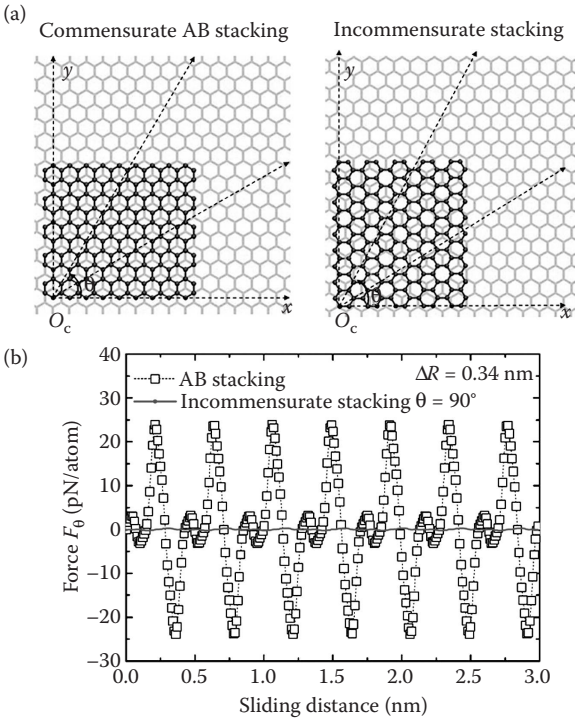

FIGURE 1.17 (a) A finite rectangular graphene flake is stacked on another graphene with AB stacking (left), and incommensurate stacking (right). The graphene fakes slide 3 nm on the lower graphene sheets along different directions θ. (b) Variation of the in-plane force F_θ acting on the perfect graphene flakes in the AB stacking and incommensurate stacking with an interlayer distance $\Delta R = 0.34$ nm when sliding along $\theta = 90°$. (With permission from Y F Guo, W L Guo and C F Chen, *Phys. Rev. B*, 76, 155429. Copyright 2007 by the American Physical Society.)

from simulations [40,41]. Small crystalline AFM tips show substantial static friction only at commensurate alignments [42]. The friction between unaligned MoS_2 crystals is extremely low in ultrahigh vacuum, but rises rapidly on exposure to air [43]. Guo and coworkers measured the friction force between a graphene flake and an infinite graphene sheet [44]. They found that the friction between AB stacking graphene layers (commensurateness) is two orders larger than the friction between incommensurate stacking graphene layers (Figure 1.17). And the friction for commensurate stacking graphene layers is stick-slip, while the friction for incommensurate stacking graphene layers is slip.

1.3 VARIOUS ATOMIC-SCALE FRICTIONAL MODELS

From the above discussions, it is clear that friction is closely related to the atomic details on the friction interface. Determining the forces required to move atoms past each other is a challenge in designing nanomachines. In 2008, scientists for the

first time were able to move a single atom across a surface, and measured the force required. Using ultrahigh vacuum and nearly zero temperature (5 K), a modified AFM was used to drag a cobalt atom, and a carbon monoxide molecule, across surfaces of copper and platinum [45]. However, before the development of the experimental setup for determining forces on a single atom, various atomic-scale frictional models have been developed for understanding the phenomena related to friction.

1.3.1 Prandtl–Tomlinson Model

The Tomlinson model [11], also known as the PT model [12], is one of the most popular models in nanotribology widely used as the basis for many investigations of frictional mechanisms on the atomic scale. Essentially, a nanotip is dragged by a spring over a corrugated energy landscape as shown in Figure 1.18. Despite its simplicity, fundamental factors controlling the atomic-scale friction are all considered: movable surface atoms, periodic surface potential, and energy dissipation from the vibration of surface atoms. Ignoring the inertial effect, total energy of the whole system is expressed by

$$E = V(x) + \frac{1}{2}k(x - X)^2, \tag{1.10}$$

where k is the spring constant. If the tip–surface interaction is described by a sinusoidal potential with amplitude V_0 and periodicity a then

$$V(x) = -\frac{V_0}{2}\cos\frac{2\pi x}{a}. \tag{1.11}$$

For the tip moving with velocity v_M, $X = v_M t$ in Equation 1.10.
The equilibrium position $x_{\min}$ of the tip is determined by

$$\frac{\partial E}{\partial x} = \frac{\pi V_0}{a}\sin\left(\frac{2\pi x}{a}\right) + k\left(x - v_M t\right) = 0. \tag{1.12}$$

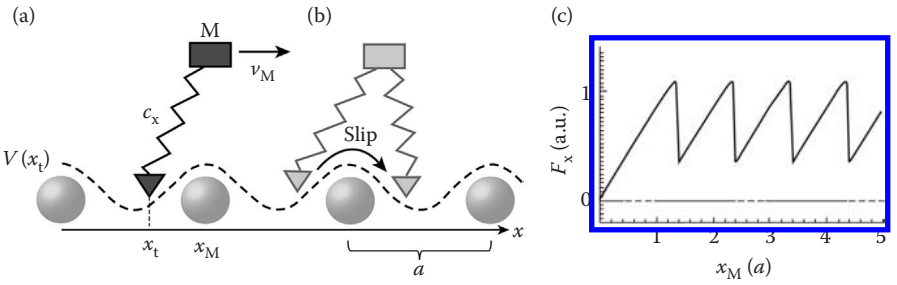

FIGURE 1.18 Prandtl–Tomlinson model. (a,b) A nanotip is dragged by a spring over a corrugated energy landscape with periodicity a. (c) The variation of friction force with the displacement of the tip.

Using the approximation $\sin(2\pi\, x/a) \approx 2\pi\, x/a$, the initial velocity of the tip is calculated to be

$$\left.\frac{dx_{\min}}{dt}\right|_{t\to 0} = \frac{v_M}{1+\eta}, \tag{1.13}$$

where η is a dimensionless number:

$$\eta = \frac{2\pi^2 V_0}{ka^2}, \tag{1.14}$$

which characterizes the ratio between the energy corrugation and the elastic energy stored in the spring. From Equation 1.12, the lateral force F_L can be obtained as

$$F_L = -k(x_{\text{tip}} - X) = \frac{\pi V_0}{a}\sin\frac{2\pi x_{\text{tip}}}{a}. \tag{1.15}$$

The above equation has the maximum value for $x_{\text{tip}} = a/4$. Thus, the relationship between the energy barrier V_0 and maximum lateral force $F_L^{\max}$ is

$$V_0 = \frac{a}{\pi}F_L^{\max}. \tag{1.16}$$

By equating the second derivative of the energy to zero

$$\frac{\partial^2 E}{\partial x^2} = \frac{2\pi^2 V_0}{a^2}\cos\left(\frac{2\pi x}{a}\right) + k = 0, \tag{1.17}$$

the instability point of the tip is obtained

$$x^* = \frac{a}{2\pi}\arccos\left(-\frac{1}{\eta}\right). \tag{1.18}$$

At the position x^* and the moment of instability $t = t^*$, the tip would jump to another local minimum energy position. This kind of motion is called "stick–slip." Substituting Equation 1.18 into Equation 1.15, the lateral force at the moment of the jump could be determined as

$$F_L^* = \frac{ka}{2\pi}\sqrt{\eta^2 - 1}. \tag{1.19}$$

Only if $\eta^2 - 1 \geq 0$, can the critical force for the occurrence of the "stick–slip" motion make sense. If $\eta > 1$, there exists two kinds of atomic mechanisms for the

"stick–slip" motion. The first kind is a purely mechanical type, that is, the mode of phonon produced in crystal and vibrator. The second kind is a purely electron type, that is, the mode of electron–hole pair excitations. If $\eta \leq 1$, the vibrator would slip continuously without energy dissipation.

1.3.2 Frenkel–Kontorova Model

As shown in Figure 1.19a, the FK model [15,16] describes the motion of a 1D atomic chain in the periodic potential. Compared to the PT model, the FK model is closer to the real behavior of atomic-scale friction. Assuming that all the atoms have the same mass m and all the springs have the same elastic constant k, the dynamic equation for any atom would be

$$m\frac{\partial^2 x_i}{\partial t^2} + \zeta\frac{\partial x_i}{\partial t} + k_1(2x_i - x_{i+1} - x_{i-1}) = -\frac{\pi V_0}{a}\sin\frac{2\pi x_i}{a}. \tag{1.20}$$

It should be noted that there are two modes for the FK model. The first is the pinned mode, in which the average velocity of the atoms is zero. The second is the sliding mode, in which the average velocity of the atoms is not zero.

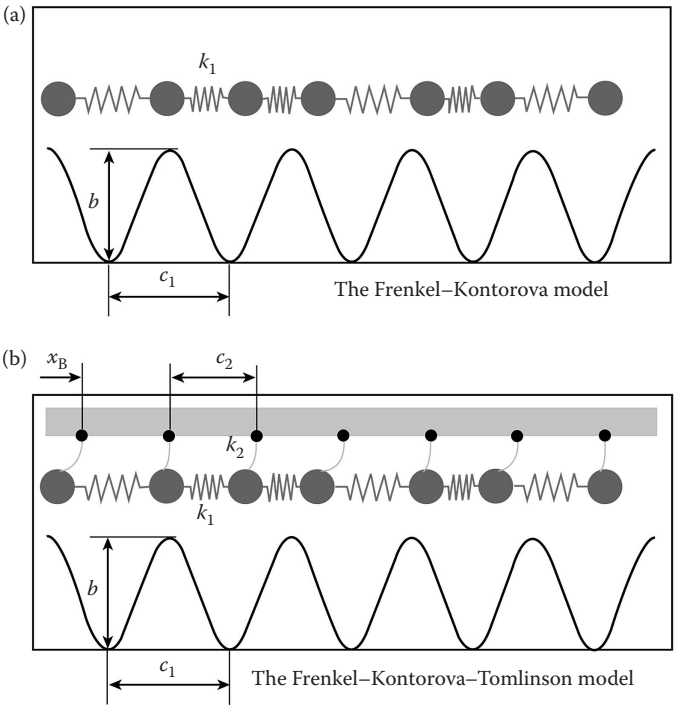

FIGURE 1.19 (a) The FK model describes the motion of a 1D atomic chain in the periodic potential. (b) The FKT model combining the advantages of FK model and PT model.

Without loss of generality, the FK model in the pinned mode can be written as

$$x_{i+1} + x_{i-1} - 2x_i + b\sin x_i + S = 0, \tag{1.21}$$

where S is the displacement induced by the external force. The general solution of the above equation is

$$x_i = -\pi + \arcsin\left(\frac{S}{b}\right) + 2\pi i, \quad S \le b. \tag{1.22}$$

The sliding model can be divided into two types. The first type is solid sliding. There are no relative movements between atoms. And the system moves like a rigid body. Thus, this type is also called "rigid sliding." The second type is uniform sliding. For this type, the system is composed of groups with different densities and average sliding velocities.

1.3.3 Frenkel–Kontorova–Tomlinson Model

Combining the advantages of FK model and PT model, Weiss and Elmer proposed the Frenkel–Kontorova–Tomlinson (FKT) model [46] as shown in Figure 1.19b. The FKT model is a 1D lattice model for the atomic monolayer of the surface of a soft body which slides on a hard body. The monolayer is described by a chain of N atoms with harmonic nearest-neighbor interactions (coil springs). The interaction of each atom with the otherwise rigid upper body is also harmonic (leaf springs). The equilibrium positions of the atoms due to these interactions define a regular lattice where the lattice constant is assumed to be the bulk lattice constant of the upper body. The interaction of the atoms with the lower body is described by a spatially periodic external potential, which represents a hard surface. The lower body is assumed to be fixed whereas the upper body is movable. The potential energy of the FKT model is

$$\begin{aligned} E(\xi_1,\cdots,\xi_N,x_B) = \frac{1}{2}\sum_{j=1}^{N}(\xi_j - \xi_{j-1})^2 + \frac{k_2}{2}\sum_{j=1}^{N}{\xi_j}^2, \\ + \frac{b}{2\pi}\sum_{j=1}^{N}\cos 2\pi(x_B + c_2 j + \xi_j) - Fx_B \end{aligned} \tag{1.23}$$

where c_2 is the lattice constant of the upper body, x_B is the position of the upper body relative to the lower body, ξ_j is the position of particle j relative to the support $x_B + c_2 j$, k_2 is the stiffness of the leaf spring, b is the strength of the external potential, and F is the force applied to the upper body. All the variables and parameters are measured in dimensionless units. They are based on the following independent basic units: The length unit is the surface lattice constant of the lower body, and the unit of the interaction strength is the stiffness of the nearest-neighbor coupling. All other units can be expressed in terms of these basic units.

For $k_2 = 0$ the FKT model becomes the FK model. For k_2, $b \to \infty$ but b/k_2 finite, or similarly by dropping the nearest-neighbor interaction, the FKT model turns into the Tomlinson model of independent oscillators.

As in the FK model, the behavior strongly depends on whether the ratio of lattice constants is commensurate or incommensurate. In the incommensurate case, Aubry's transition by breaking of analyticity also appears in the FKT model. The behavior depends strongly on the strength of the interaction between the sliding surfaces. For increasing interaction, three thresholds are found which denote the appearance of static friction, of kinetic friction in the quasistatic limit, and of metastable states in that order. These are identical only in the incommensurate case. In the commensurate case, static friction can be nonzero even though the kinetic friction vanishes for sliding velocity going to zero.

1.3.4 Variable Density Frenkel–Kontorova Model

To investigate the boundary slip in nanoflow, Lichter and coworkers proposed the variable density FK (vdFK) model [47–49]. The vdFK model describes the first liquid layer adjacent to the solid surface. According to this model, the dynamic equation for atom i in the first liquid layer is

$$m\frac{\partial^2 x_i}{\partial t^2} = -\frac{\pi V_0}{a}\sin\left(\frac{2\pi x_i}{a}\right) + k(x_{i+1} - 2x_i + x_{i-1}) + \eta_{LL}\left(v - \frac{\partial x_i}{\partial t}\right) - \eta_{LS}\frac{\partial x_i}{\partial t}. \tag{1.24}$$

In the above equation, the left term represents the inertial force exerted on atom i in the first liquid layer. The first term on the right hand of the equation is the interaction force between atom i and the solid surface, the second term is the spring force between adjacent atoms in the first layer, the third term is the force exerted by the molecules from other layer to atom i in the first layer (η_{LL} is the bulk viscosity of the liquid) and the last term is the friction force between the first layer of liquid and the solid surface due to boundary slip (η_{LS} is the coefficient of friction).

1.4 VELOCITY-DEPENDENT FRICTIONAL MODEL AND ITS PHYSICAL ORIGIN

When it comes to the atomic-scale friction, there are many different laws. In particular, it has been known that the friction force between two macroscopic objects is independent of their relative velocity as was suggested by Coulomb. However, the friction force on the nanoscale is found to be velocity dependent, which makes things much more complicated [50].

Experimental results conducted for the velocities in the range of 1 nm/s ~ 1 μm/s always showed a logarithmic increase in friction with velocity [51–54] between a tip and sample surfaces as shown in Figure 1.20. Gnecco et al. [52] attributed this phenomenon to the temperature effects and combined the PT model with the rate theory

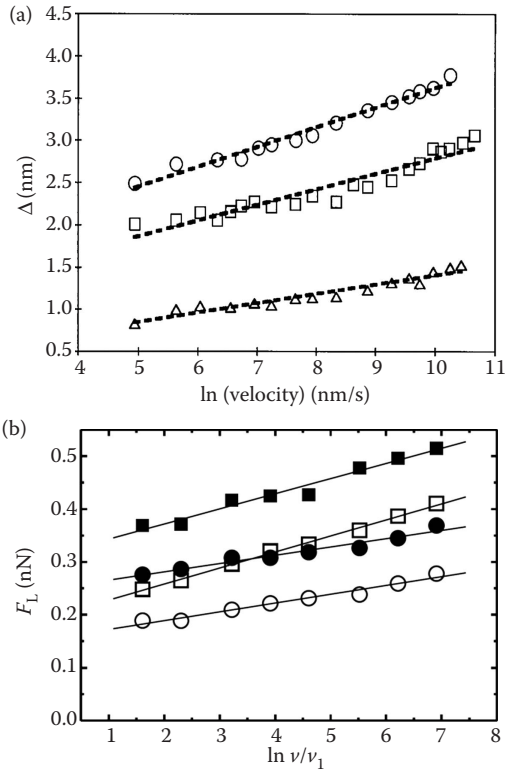

FIGURE 1.20 (a) Fits and experimental data of friction versus tip velocity for the organosilanes grafted on silica and probed with three cantilevers: k_2 (triangle), k_1 (square), and k_{3a} (circle). (With permission from T Bouhacina et al., *Phys. Rev. B*, 56, 7694–7703. Copyright (1997) by the American Physical Society.) (b) Sliding friction between the tip of a friction force microscope and NaCl(100) as a function of the scanning velocity at $F_N = 0.44$ nN (circles) and $F_N = 0.65$ nN (squares) loads. Open and solid symbols refer to the mean absolute value of the lateral force maps $\langle F_L \rangle$ and the mean absolute value of the peaks in the friction loops $\langle F_{L,\,\max} \rangle$, respectively. (With permission from E Gnecco et al., *Phys. Rev. Lett.*, 84, 1172–1175. Copyright 2000 by the American Physical Society.)

to give explanations. At zero temperature, the tip does not jump until the energy barrier $\Delta E = 0$, that is, when the condition obtained from Equation 1.18 is satisfied. At a finite temperature T, the tip can jump even if $\Delta E \neq 0$. This is because thermal energy of the tip can assist it to jump out of the potential well where it is confined with a characteristic frequency f_0. The probability p that the tip does not jump changes with time according to the rate theory

$$\frac{\mathrm{d}p(t)}{\mathrm{d}t} = -f_0 \exp\left(-\frac{\Delta E(t)}{k_\mathrm{B}T}\right) p(t), \tag{1.25}$$

where ΔE is a function of time, k_B is the Boltzmann constant. To obtain the lateral force corresponding to the maximum jump probability, a change of variable replacing time by corresponding lateral force is made

$$\frac{dp(F_L)}{dF_L} = -f_0 \exp\left(-\frac{\Delta E(F_L)}{k_B T}\right)\left(\frac{dF_L}{dt}\right)^{-1} p(F_L). \tag{1.26}$$

Assuming that the energy barrier ΔE decreases linearly with the lateral force F_L, and noting that $dF_L/dt \cong kv$, where k is the effective stiffness of the system and v is the sliding velocity, the relation between friction force and velocity is obtained

$$F_L(v) = F_{L0} + \frac{k_B T}{\lambda} \ln \frac{v}{v_1}, \tag{1.27}$$

where λ is a characteristic length on the order of the lattice constant a.

However, Tambe and Bhushan [55] found that the dependence of friction on velocity is not necessarily logarithmic for velocities up to the order of 1 mm/s. The nanoscale friction force between two contacting surfaces is a result of three components: interfacial adhesion between contacting asperities, the energy required for deformation of contacting asperities during relative motion and stick–slip. At different relative sliding velocities, different components dominate the friction as shown in Figure 1.21. For example, the atomic stick–slip contribution is most important in the low-velocity regime, which results in the logarithmic dependence of friction on velocity as we have discussed above.

1.5 DIFFUSIVE AND BALLISTIC FRICTION

Most of the discussions above was about the friction between a dragged tip and the surface. However, the friction of adsorbed molecules or mobile clusters thermally diffusing on surfaces is also important and of interest [56–58]. In this case, the behavior of the adsorbate is determined by the competition between the potential energy barrier induced by the adsorbate–substrate interactions and the kinetic energy of the adsorbate.

Guerra and coworkers [56,57] simulated the motion of gold clusters with different initial velocities on graphite surface as shown in Figure 1.22. The frictional sliding of the gold clusters illustrates two distinct nanofriction regimes: a standard diffusive friction at low speed, and a new ballistic one at high speed, where the effect of temperature on friction is opposite. Angular motion and rotations cannot be ignored and are crucial to both diffusive and ballistic regimes. The interplay between translations and rotations, besides turning ballistic trajectories from straight to curved, controls the crossover between the two sliding regimes. Translational and rotational stops and starts, strictly correlated in diffusion and drift, become anticorrelated in fast ballistic sliding. Ballistic friction, although quite different from diffusive friction and naturally erratic in small clusters, is still viscous in its speed dependence, a useful result

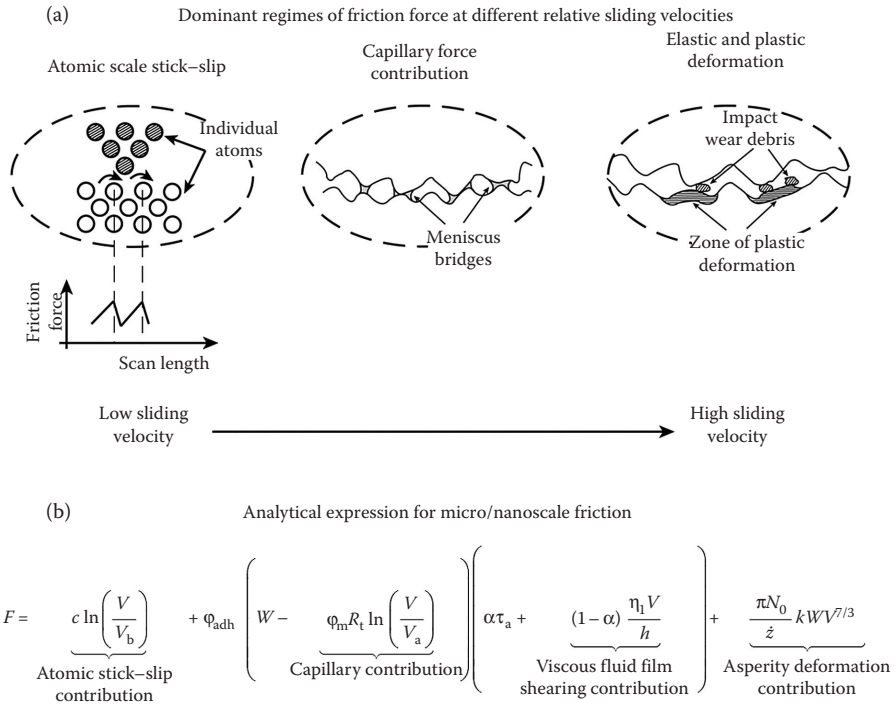

FIGURE 1.21 (a) Schematic diagram illustrating various dominant regimes of the friction force at different relative sliding velocities from atomic scale stick–slip at low velocities to deformation-related energy dissipation at high velocities. (b) Comprehensive analytical expression for the velocity dependence of nanoscale friction with the dominant friction mechanisms. (Adapted from N S Tambe and B Bhushan. *Nanotechnology*, 16, 2309–2324, 2005.)

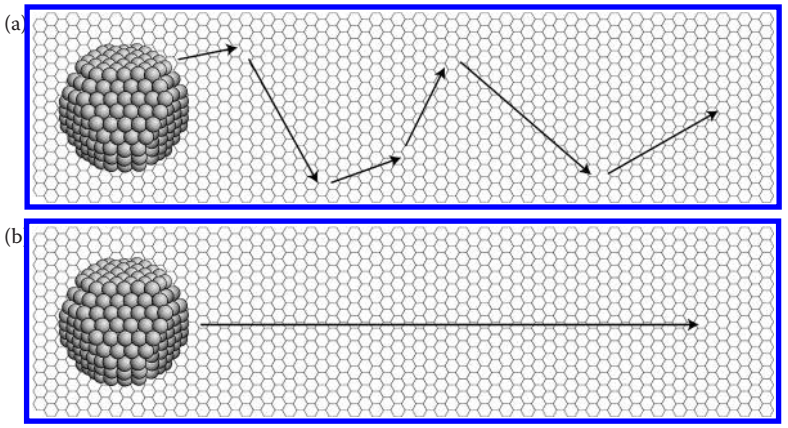

FIGURE 1.22 Surfing of gold clusters on graphite. (a) Diffusive friction; (b) ballistic friction. (With permission from Macmillan Publishers Ltd. *Nat. Mater.*, A Schirmeisen. Nanofriction: Surfing on graphite waves, 9, 615–616, copyright 2010.)

not discounted in principle for this and other systems, which would be interesting to pursue and test experimentally.

In the diffusive regime, the adsorbate may behave differently under different conditions. The motion of the adsorbate is controlled by the Langevin equation (LE), in which there are two phenomenological parameters: the potential energy barrier E_a and the kinetic friction coefficient η. Solutions of the LE have shown four distinct regimes of surface diffusion [59,60]: regime I (single jumps), where the E_a is strong, and the η is high, the adsorbate jumps from one minimum to a neighboring minimum; regime II (multiple jumps), where the E_a is strong, and the η is low, the adsorbate may jump from one minimum to a distant local minimum; regime III (quasi-continuous Brownian motion), where the E_a is weak, and the η is high, the adsorbate moves continuously similar to that of a Brownian particle in high-friction liquid; regime IV (ballistic-like Brownian motion), where the E_a is weak, and the η is low, the adsorbate moves continuously and travels in linear trajectories at picosecond time scale, which is similar to that of a Brownian particle in a low-friction liquid. Jafary-Zadeh and coworkers [58] investigated the thermally induced motion of C_{60} on the graphene substrate with a shallow potential energy surface. The C_{60} molecule exhibits a quasi-continuous Brownian motion in the temperature range of 25–75 K, then follows a ballistic-like Brownian motion at temperatures above 75 K.

1.6 SUMMARY AND CONCLUSIONS

Friction is an issue related to two rubbing surfaces, which seemingly is simple, but actually is a complex problem. Uncovering the underlying mechanisms of friction requires both the development of physical theories and experimental techniques. This manuscript reviewed selected publications on friction and mainly focused on the physical mechanisms of atomic-scale friction. A brief look at the development history of friction was given first, from basic laws of friction to recent progresses on atomic-scale friction. Considering the important role of the structure of the rubbing surfaces and adsorbed lubricant films, we discussed the commensurate and incommensurate interfaces and their influence on the behavior of friction in Section 1.2. In order to understand the mechanisms of friction from the point of view of intermolecular interactions, various atomic-scale friction models have been established, which are summarized in Section 1.3. Theoretical and experimental researches conducted to explore the velocity-dependent frictional behavior and its physical origin were reviewed in Section 1.4. In the end, the diffusive and ballistic friction of adsorbed molecules or mobile clusters thermally moving on surfaces were presented.

With the development of experimental techniques and simulation methods on the atomic scale, the field of atomic-scale friction has been developing fast in recent years and several applications have been achieved or are about to be achieved. However, the mechanism behind the phenomena related to atomic-scale friction is yet to be clearly understood. In particular, we would like to mention the following issues:

- In recent years, water-based lubricant and superlubricity have attracted considerable interest [61–64], which is closely related to the adsorbate between the two rubbing surfaces. The adsorbate may experience phase transitions or

even chemical reactions in response to the variation of external conditions, which in turn influences the friction. This requires further experimental investigations related to chemical reactions or MD simulations employing the Reax force field [65], which can simulate a chemical reaction.

- The atomic-scale frictional models developed so far were mostly 1D. To capture all the characteristics of the real frictional system, further extension of the 1D model to 2D is deserved.
- Friction is not only closely related to the intermolecular interactions, but also to electron transfer because the rubbing materials may become electrically charged through friction. Thus, friction is a typical multiscale problem, which should be solved through multiscale methods, such as *ab initio* MD [66,67] or QM/MM hybrid method [68–72]. The developers of QM/MM, Martin Karplus, Michael Levitt and Arieh Warshel, have won the 2013 Nobel Prize in Chemistry for the development of multiscale models for complex chemical systems.

In conclusion, friction, as a mechanical problem, is of great importance where physics, chemistry, and surface science intersect. The solution of this old problem could, in turn, promote the development of these subjects.

NOMENCLATURE

A	Contact area
a	Distance
E	Energy
ε	Potential well depth for LJ potential
F	Force
H	Hamiltonian of the system
p	Probability
S	Displacement
t	Time
T	Temperature
V	Potential energy
v	Velocity
x	Coordinate
λ	Length
μ	Friction coefficient
σ	Distance at which LJ potential is zero
τ	Shear strength

ACKNOWLEDGMENTS

This work was jointly supported by the National Natural Science Foundation of China (NSFC, Grant 11202213 and 11072244), the Key Research Program of the Chinese Academy of Sciences (Grant KJZD-EW-M01), and the Instrument Developing Project of the Chinese Academy of Sciences (Grant Y2010031).

REFERENCES

1. G Amontons, De la résistance causée dans les machines (On the resistance originating in machines). *Mem. Acad. Roy. Sci. (Proceedings of the French Royal Academy of Sciences)*, 206–226, 1699.
2. F P Bowden and D Tabor. *The Friction and Lubrication of Solids*. Clarendon Press, Oxford, 1950.
3. H Kanamori. Mechanics of earthquakes. *Annu. Rev. Earth Planet. Sci.*, 22, 207–237, 1994.
4. F P Bowden and L Leben. The nature of sliding and the analysis of friction. *Proc. R. Soc. London Series A-Math. Phys. Eng. Sci.*, 169, 371–391, 1939.
5. M Urbakh, J Klafter, D Gourdon and J Israelachvili. The nonlinear nature of friction. *Nature*, 430, 525–528, 2004.
6. C H Scholz. Earthquakes and friction laws. *Nature*, 391, 37–42, 1998.
7. Y F Mo, K T Turner, and I Szlufarska. Friction laws at the nanoscale. *Nature*, 457, 1116–1119, 2009.
8. M Cieplak, E D Smith, and M O Robbins. Molecular-origins of friction—The force on adsorbed layers. *Science*, 265, 1209–1212, 1994.
9. W M Miller, D M Tanner, S L Miller, and K A Peterson. MEMS reliability: The challenge and the promise. *Proceedings of 4th Annual "The Reliability Challenge"*, Dublin, Ireland, pp. 4.1–4.7, 1998.
10. D M Tanner, J A Walraven, L W Irwin, M T Dugger, N F Smith, W P Eaton, W M Miller, and S L Miller. The effect of humidity on the reliability of a surface micromachined microengine. *Proceedings of IEEE International Reliability Physics Symposium*, San Diego CA, pp. 189–197, 1999.
11. G A Tomlinson. A molecular theory of friction. *Philos. Mag.*, 7, 905–939, 1929.
12. L Prandtl. Ein gedankenmodell zur kinetischen theorie der festen körper (A Conceptual Model to the Kinetic Theory of Solid Bodies). *Z. Angew. Math. Mech. (Journal of Applied Mathematics and Mechanics)*, 8, 85–106, 1928.
13. V L Popov. *Contact Mechanics and Friction*. Springer, Berlin, 2010.
14. V L Popov and J A T Gray. Prandtl–Tomlinson model: History and applications in friction, plasticity, and nanotechnologies. *ZAMM-Z. Angew. Math. Mech.*, 92, 683–708, 2012.
15. T A Kontorova and Y I Frenkel. On the theory of plastic deformation and twinning, Part I. *Zh. Eksp. Teor. Fiz. (J. Exp. Theor. Phys. (JETP))*, 8, 89–95, 1938.
16. T A Kontorova and Y I Frenkel. On the theory of plastic deformation and twinning, Part II. *Zh. Eksp. Teor. Fiz. (J. Exp. Theor. Phys. (JETP))*, 8, 1340–1348, 1938.
17. O M Braun and Y S Kivshar. *The Frenkel–Kontorova Model: Concepts, Methods and Applications*. Springer, New York, 2004.
18. N S Tambe and B Bhushan. Identifying materials with low friction and adhesion for nanotechnology applications. *Appl. Phys. Lett.*, 86, 061906, 2005.
19. N S Tambe and B Bhushan. Nanoscale friction and wear maps. *Philos. Trans. R. Soc. A-Math. Phys. Eng. Sci.*, 366, 1405–1424, 2008.
20. M Lucas, X H Zhang, I Palaci, C Klinke, E Tosatti, and E Riedo. Hindered rolling and friction anisotropy in supported carbon nanotubes. *Nat. Mater.*, 8, 876–881, 2009.
21. W D Luedtke and U Landman. Slip diffusion and Levy flights of an adsorbed gold nanocluster. *Phys. Rev. Lett.*, 82, 3835–3838, 1999.
22. D W Brenner. Empirical potential for hydrocarbons for use in simulating the chemical vapor-deposition of diamond films. *Phys. Rev. B*, 42, 9458–9471, 1990.
23. A N Kolmogorov and V H Crespi. Registry-dependent interlayer potential for graphitic systems. *Phys. Rev. B*, 71, 235415, 2005.
24. P Bak. Commensurate phases, incommensurate phases and the devil's staircase. *Rep. Prog. Phys.*, 45, 587–629, 1982.

25. F C Frank and J H Van der Merwe. One-dimensional dislocations. II. Misfitting monolayers and oriented overgrowth. Proc. R. Soc. London Series A-Math. *Phys. Eng. Sci.*, 198, 216–225, 1949.
26. S Aubry. Defectibility and frustration in incommensurate structures—The devil's stair case transformation. *Ferroelectrics*, 24, 53–60, 1980.
27. P Bak and V L Pokrovsky. Theory of metal–insulator-transition in peierls systems with nearly half-filled bands. *Phys. Rev. Lett.*, 47, 958–961, 1981.
28. M H Müser. Nature of mechanical instabilities and their effect on kinetic friction. *Phys. Rev. Lett.*, 89, 224301, 2002.
29. A Hodgson and S Haq. Water adsorption and the wetting of metal surfaces. *Surf. Sci. Rep.*, 64, 381–451, 2009.
30. I F Lyuksyutov, A G Naumovets, and V Pokrovsky. *Two-Dimensional Crystals*. Academic Press, Boston, 1992.
31. B N J Persson. Ordered structures and phase-transitions in adsorbed layers. *Surf. Sci. Rep.*, 15, 1–135, 1992.
32. O M Braun and A G Naumovets. Nanotribology: Microscopic mechanisms of friction. *Surf. Sci. Rep.*, 60, 79–158, 2006.
33. T Masuda, C J Barnes, P Hu, and D A King. Frenkel–Kontorova domain-wall phase-transitions in an adsorbed layer—potassium on Co{101̄0}. *Surf. Sci.*, 276, 122–138, 1992.
34. B V Andryushechkin, K N Eltsov, and V M Shevlyuga. Atomic scale observation of iodine layer compression on Cu(111). *Surf. Sci.*, 472, 80–88, 2001.
35. E D Smith, M O Robbins, and M Cieplak. Friction on adsorbed monolayers. *Phys. Rev. B*, 54, 8252–8260, 1996.
36. G He, M H Muser, and M O Robbins. Adsorbed layers and the origin of static friction. *Science*, 284, 1650–1652, 1999.
37. M H Müser and M O Robbins. Conditions for static friction between flat crystalline surfaces. *Phys. Rev. B*, 61, 2335–2342, 2000.
38. J Krim, D H Solina, and R Chiarello. Nanotribology of a Kr monolayer—a quartz-crystal microbalance study of atomic-scale friction. *Phys. Rev. Lett.*, 66, 181–184, 1991.
39. C Mak and J Krim. Quartz-crystal microbalance studies of the velocity dependence of interfacial friction. *Phys. Rev. B*, 58, 5157–5159, 1998.
40. B N J Persson and A Nitzan. Linear sliding friction: On the origin of the microscopic friction for Xe on silver. *Surf. Sci.*, 367, 261–275, 1996.
41. M S Tomassone, J B Sokoloff, A Widom, and J Krim. Dominance of phonon friction for a xenon film an a silver (111) surface. *Phys. Rev. Lett.*, 79, 4798–4801, 1997.
42. M Hirano, K Shinjo, R Kaneko, and Y Murata. Observation of superlubricity by scanning tunneling microscopy. *Phys. Rev. Lett.*, 78, 1448–1451, 1997.
43. J M Martin, C Donnet, T Lemogne, and T Epicier. Superlubricity of molybdenum-disulfide. *Phys. Rev. B*, 48, 10583–10586, 1993.
44. Y F Guo, W L Guo, and C F Chen. Modifying atomic-scale friction between two graphene sheets: A molecular-force-field study. *Phys. Rev. B*, 76, 155429, 2007.
45. M Ternes, C P Lutz, C F Hirjibehedin, F J Giessibl, and A J Heinrich. The force needed to move an atom on a surface. *Science*, 319, 1066–1069, 2008.
46. M Weiss and F J Elmer. Dry friction in the Frenkel–Kontorova–Tomlinson model: Static properties. *Phys. Rev. B*, 53, 7539–7549, 1996.
47. S Lichter, A Roxin and S Mandre. Mechanisms for liquid slip at solid surfaces. *Phys. Rev. Lett.*, 93, 086001, 2004.
48. A Martini, H Y Hsu, N A Patankar, and S Lichter. Slip at high shear rates. *Phys. Rev. Lett.*, 100, 206001, 2008.
49. A Martini, A Roxin, R Q Snurr, Q Wang, and S Lichter. Molecular mechanisms of liquid slip. *J. Fluid Mech.*, 600, 257–269, 2008.

50. E Gnecco and E Meyer. *Fundamentals of Friction and Wear*. Springer-Verlag, Berlin, 2007.
51. T Bouhacina, J P Aime, S Gauthier, D Michel, and V Heroguez. Tribological behavior of a polymer grafted on silanized silica probed with a nanotip. *Phys. Rev. B*, 56, 7694–7703, 1997.
52. E Gnecco, R Bennewitz, T Gyalog, C Loppacher, M Bammerlin, E Meyer, and H J Guntherodt. Velocity dependence of atomic friction. *Phys. Rev. Lett.*, 84, 1172–1175, 2000.
53. E Gnecco, R Bennewitz, T Gyalog, and E Meyer. Friction experiments on the nanometre scale. *J. Phys.: Condens. Matter*, 13, R619–R642, 2001.
54. E Riedo, E Gnecco, R Bennewitz, E Meyer, and H Brune. Interaction potential and hopping dynamics governing sliding friction. *Phys. Rev. Lett.*, 91, 084502, 2003.
55. N S Tambe and B Bhushan. Friction model for the velocity dependence of nanoscale friction. *Nanotechnology*, 16, 2309–2324, 2005.
56. R Guerra, U Tartaglino, A Vanossi, and E Tosatti. Ballistic nanofriction. *Nat. Mater.*, 9, 634–637, 2010.
57. A Schirmeisen. Nanofriction: Surfing on graphite waves. *Nat. Mater.*, 9, 615–616, 2010.
58. M Jafary-Zadeh, C D Reddy, V Sorkin, and Y W Zhang. Kinetic nanofriction: A mechanism transition from quasi-continuous to ballistic-like Brownian regime. *Nanoscale Res. Lett.*, 7, 148, 2012.
59. T Alanissila and S C Ying. Universal properties of classical surface-diffusion. *Phys. Rev. Lett.*, 65, 879–882, 1990.
60. T Ala-Nissila, R Ferrando, and S C Ying. Collective and single particle diffusion on surfaces. *Adv. Phys.*, 51, 949–1078, 2002.
61. J B Luo, M W Shen, and S Z Wen. Tribological properties of nanoliquid film under an external electric field. *J. Appl. Phys.*, 96, 6733–6738, 2004.
62. J J Li, L R Ma, S H Zhang, C H Zhang, Y H Liu, and J B Luo. Investigations on the mechanism of superlubricity achieved with phosphoric acid solution by direct observation. *J. Appl. Phys.*, 114, 114901, 2013.
63. L Sun, C H Zhang, J J Li, Y H Liu, and J B Luo. Superlubricity of Si3N4 sliding against SiO_2 under linear contact conditions in phosphoric acid solutions. *Sci. China-Technol. Sci.*, 56, 1678–1684, 2013.
64. D W Zhao, Y Y He, T Q Wang, X C Lu, and J B Luo. Wafer bending/orientation characterization and their effects on fluid lubrication during chemical mechanical polishing. *Tribol. Int.*, 66, 330–336, 2013.
65. K Chenoweth, A C T van Duin, and W A Goddard. ReaxFF reactive force field for molecular dynamics simulations of hydrocarbon oxidation. *J. Phys. Chem. A*, 112, 1040–1053, 2008.
66. R Car and M Parrinello. Unified approach for molecular-dynamics and density-functional theory. *Phys. Rev. Lett.*, 55, 2471–2474, 1985.
67. J L Zang, Q Z Yuan, F C Wang, and Y P Zhao. A comparative study of Young's modulus of single-walled carbon nanotube by CPMD, MD and first principle simulations. *Comput. Mater. Sci.*, 46, 621–625, 2009.
68. A Warshel and M Levitt. Theoretical studies of enzymic reactions: Dielectric, electrostatic and steric stabilization of the carbonium ion in the reaction of lysozyme. *J. Mol. Biol.*, 103, 227–249, 1976.
69. C Chothia, A M Lesk, A Tramontano, M Levitt, S J Smithgill, G Air, S Sheriff, et al. Conformations of immunoglobulin hypervariable regions. *Nature*, 342, 877–883, 1989.
70. W Yang, R Bitetti-Putzer, and M Karplus. Chaperoned alchemical free energy simulations: A general method for QM, MM, and QM/MM potentials. *J. Chem. Phys.*, 120, 9450–9453, 2004.
71. J Yin and Y P Zhao. Hybrid QM/MM simulation of the hydration phenomena of dipalmitoyl phosphatidyl choline head group. *J. Colloid Interface Sci.*, 329, 410–415, 2009.
72. Y P Zhao. *Physical Mechanics of Surface and Interface*. Science Press, Beijing, 2012.